Carbon Materials

DOI: 10.1002/ange.200703864

Theoretical Model for Nanoporous Carbon Supercapacitors**

Jingsong Huang, Bobby G. Sumpter, and Vincent Meunier*

Supercapacitors based on nanoporous carbon materials, commonly called electric double-layer capacitors (EDLCs), have recently attracted considerable attention.[1,2] Carbon supercapacitors bridge the gap between batteries and conventional dielectric capacitors, and are ideal for the rapid storage and release of energy. To develop supercapacitors as an alternative to batteries, currently intense research efforts aim at increasing the energy density by optimizing the pore size distribution of nanoporous carbon materials. In their breakthrough work, Gogotsi and co-workers[3] synthesized carbide-derived carbons with unimodal micropores[4] smaller than 1 nm, and found that these new materials exhibit an anomalous increase in capacitance compared to others with pore sizes above 2 nm. These results challenge the long-held presumption that pores smaller than the size of solvated electrolyte ions do not contribute to energy storage. Herein, we present an explanation for the anomalous increase in capacitance for pores below 1 nm and for the slightly increasing capacitance with increasing pore size above 2 nm by using a heuristic theoretical model and first-principles density functional theory (DFT) calculations.

Generally it is assumed that the capacitance of EDLCs follows that of a parallel-plate capacitor:[2]

$$C = \frac{\varepsilon_r \varepsilon_0 A}{d} \text{ or } C/A = \frac{\varepsilon_r \varepsilon_0}{d} \quad (1)$$

where ε_r is the electrolyte dielectric constant, ε_0 is the permittivity of a vacuum, A is the electrode specific surface area, and d is the effective thickness of the electric double layer (the Debye length). Assuming a planar pore surface, Gogotsi and co-workers[3] found that the normalized capacitance of the micropores (C/A) is proportional to the reciprocal radius of the micropores ($1/d$).[5] This finding appears to be in good agreement with Equation (1), showing the dominance of the $1/d$ term compared to the pore curvature. However, a close inspection reveals that the intercept of the linear fit is not zero (see Figure S1 in the Supporting Information). There is still a lack of a good model for nanoporous carbon supercapacitors. What happens inside the nanoconfined space within the pores is not fully understood; the effects of pore size distribution, A, and d on C are still not clear.[6–8]

Moving beyond the planar capacitor model, it seems reasonable to include the influence of pore curvature to describe the capacitance of carbon supercapacitors. Nanoporous materials can have various pore shapes, such as cylindrical, slit, and spherical types.[9] Mesoporous carbon materials obtained by template methods usually have wormhole structures.[6,10] Cylindrical pores are usually the assumption for theoretical treatments for physical adsorption of gases[11] and impedance spectroscopy.[12] Assuming cylindrical mesopores, solvated counterions enter pores and approach the pore walls to form electric double-cylinder capacitors (EDCCs; Figure 1 a). The double-cylinder capacitance is given as:[13]

$$C = \frac{2\pi\varepsilon_r \varepsilon_0 L}{\ln(b/a)} \text{ or } C/A = \frac{\varepsilon_r \varepsilon_0}{b\ln(b/(b-d))} \quad (2)$$

where L is the pore length and b and a are the radii of the outer and inner cylinders, respectively. For micropores, however, the small pores do not allow the formation of a double cylinder. Assuming cylindrical micropores, (solvated or desolvated) counterions enter the pores and line up to form electric wire-in-cylinder capacitors (EWCCs; Figure 1 b). Although the molecular geometries of the counterions might be anisotropic, the pore walls experience the average effect owing to the room-temperature rotation/translation of the counterions with respect to or along the pore axes, leading to an inner cylinder; conversely, the counterions experience the average effect if the micropore shape is slightly distorted

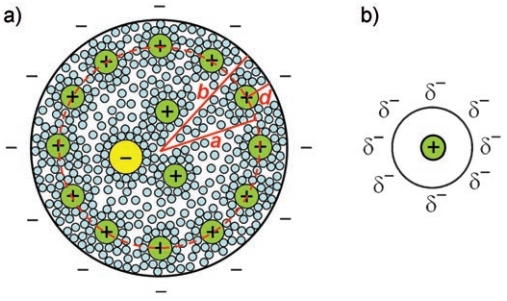

Figure 1. Schematic diagrams (top views) of a) a negatively charged mesopore with cations approaching the pore wall to form an electric double-cylinder capacitor with radii b and a for the outer and inner cylinders, respectively, separated by a distance d and b) a negatively charged micropore of radius b with cations of radius a_0 lining up to form an electric wire-in-cylinder capacitor.

[*] Dr. J. Huang, Dr. B. G. Sumpter, Dr. V. Meunier
Oak Ridge National Laboratory
Oak Ridge, TN 37831-6367 (USA)
Fax: (+1) 865-574-0680
E-mail: huangj3@ornl.gov

[**] This research was sponsored by the Laboratory Directed Research and Development Program of Oak Ridge National Laboratory (ORNL) and by the Division of Materials Sciences and Engineering, U.S. Department of Energy under Contract No. DEAC05-00OR22725 with UT-Battelle, LLC at ORNL. We are indebted to Dr. Sheng Dai, Dr. Nancy J. Dudney, and Prof. Dr. Miklos Kertesz for their helpful discussions on pore shape, electrochemical aspects, and charge transfer from molecules inside nanotubes to nanotubes, respectively.

Supporting information for this article is available on the WWW under http://www.angewandte.org or from the author.

from a cylinder, leading to an outer cylinder. In a way, EWCCs can be also viewed as EDCCs, but the key quantity for EWCCs is no longer d but rather the radius of the inner cylinder a_0, which is the effective size of the counterions (that is, the extent of electron density around the ions). By using a_0, Equation (2) becomes:

$$C/A = \frac{\varepsilon_r \varepsilon_0}{b \ln(b/a_0)} \quad (3)$$

Equations (2) and (3) are used to fit the experimental data in the third figure of reference [3] in the mesopore and micropore regions, respectively.

The experimental data in Figure 2 were obtained from references [3], [6], and [7]. For consistency, three data points from reference [7] were recalculated using the specific surface area of the electrode instead of the powder. First, we fit all of

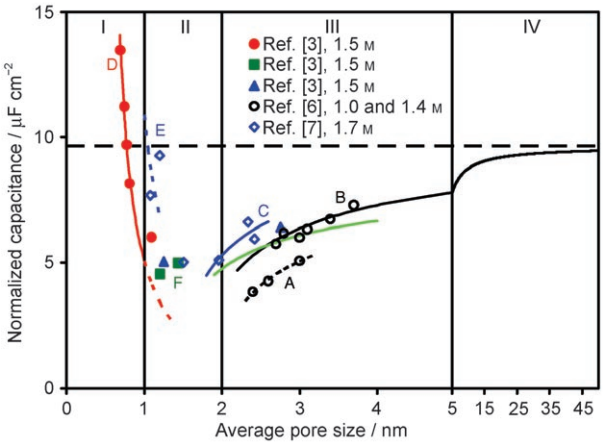

Figure 2. Experimental data of references [3], [6], and [7] fit by Equation (2) (in region III) and Equation (3) (in region I); the extrapolation of the curve in region III into region IV approaches the broken line calculated by Equation (1) using the same parameters as obtained from region III. Data are divided into six groups (A–F) for detailed analysis as described in the text. The blue dashed curve is not a result of fitting, but is shown as a visual guide.

the mesoporous data in region III using Equation (2), where it is reasonable to approximate the pores as a cylinder type. The green curve reproduces the trend of slightly increasing capacitance with increasing pore size, albeit the goodness of fit R^2 is only 0.259. The challenge to fit all data well comes from the different conditions employed in the three experiments. These carbon materials have contributions to capacitance from both micropores and mesopores,[6,7] thus hampering the application of one set of parameters in the theoretical model. In addition, carbon morphology might be different for carbon materials obtained by different methods.[2] The electrolyte in reference [7] is tetraethylammonium methylsulfonate (TEAMS) in acetonitrile (ACN) while the electrolyte in references [3] and [6] is tetraethylammonium tetrafluoroborate ($TEABF_4$) in ACN. Finally, the concentrations are different, ranging from 1.0,[6] 1.4,[6] and 1.5[3] to 1.7 M[7] (Figure 2; Table 1). To fit the experimental results well, it is necessary to subdivide the data to take into account the differences in experimental conditions. Noticing that the data of 1.7 M concentration is on the top, and the single data point of 1.5 M concentration is in the middle between 1.7 and 1.0 (1.4) M, we break down the data to fit them by concentration. The data in reference [6] were obtained from 1.0 and 1.4 M $TEABF_4$ in ACN, but the specific concentrations were not described.[2a,6] We tentatively assign group A to 1.0 M and group B to 1.4 M on the basis of the typical trend.[8a] The only data point from reference [3] in region III is included in group B for analysis because 1.5 M is close to 1.4 M. These respective fittings produce much better R^2 values (Table 1).

Table 1: Fitting results for the experimental data in regions I and III using Equations (3) and (2), respectively. Depending on the various experimental conditions in references [3], [6], and [7], experimental data are subdivided into several groups for detailed analysis.

Data group	Region	Electrolyte	Conc. [M]	R^2	ε_r	d [Å]	a_0 [Å]
A[a]	III	$TEABF_4$	1.0[b]	0.993	9.65	10.15	–
B[a]	III	$TEABF_4$	1.4,[b] 1.5[c]	0.737	9.63	8.86	–
C[d]	III	TEAMS	1.7	0.693	8.64	7.64	–
A, B, and C	III	$TEABF_4$, TEAMS	1.0, 1.4, 1.5, 1.7	0.259	6.49	7.01	–
D[c]	I	$TEABF_4$	1.5	0.985	2.23	–	2.30

[a] Reference [6]. [b] Specific concentrations of 1.0 and 1.4 M were not given in reference [6], but groups A and B are tentatively assigned to 1.0 and 1.4 M, respectively (see the text). [c] Reference [3]. [d] Reference [7].

As can be seen from Table 1, the d values are on the same order of magnitude as the calculated solvated ion radii of $TEA^+ \cdot 7ACN$ (6.5 Å) and $BF_4^- \cdot 9ACN$ (5.8 Å),[14] and the Debye length of $TEABF_4$ in ACN (6.6 Å), estimated from impedance spectroscopy.[8a] One also notices a trend from Table 1 that d increases with decreasing concentration, showing the increasing effective Debye screening length with dilution.[8a] The dielectric constant from the fitting is about 9, which is much smaller than the value of 36 for the bulk of ACN at room temperature.[15] It has been found that the dielectric constant of aqueous solution decreases in electric double layers and confined spaces.[1a,16] The limited number of data points for groups A and C puts the reliability of the fitting results into question, but we stress that the model describes the trend correctly not only for the data after being subdivided into three groups but for the data as a whole group. Further experimental studies using one electrolyte solution of various concentrations are encouraged for carbon supercapacitors with narrow mesopore size distribution.

The extrapolation of the curve for group B into region IV shows that the curve approaches asymptotically the broken line calculated by Equation (1) using the same parameters ε_r and d as in group B. In fact, Equation (2) for EDCCs can be reduced to Equation (1) for EDLCs using Taylor's expansion for large pores when $d \ll a$ (see the Supporting Information). This result indicates that the curvature plays a significant role for the capacitance of mesopores, but not for that of macropores, which can be approximated by parallel-plate capacitors. The broken line represents the limiting value of normalized capacitance for large pores at the concentration of 1.5 M.

Going down in size to micropores, especially below 1 nm, we fit group D in region I with Equation (3), reproducing the anomalous increase in capacitance. The ε_r value of 2.23 is very close to the vacuum value of 1, which is reasonable because the space between counterions and pore walls is not an absolute vacuum but has some finite electron density. This shows that the solvation shell of the counterions is completely removed, as suggested by Vix-Guterl et al.[6] The a_0 value of 2.3 Å agrees with our DFT calculations on the radial charge distribution of TEA^+ and BF_4^-, as shown below. Gogotsi and co-workers[3] also calculated the specific surface area by the nonlinear density functional theory (NLDFT) method[17] assuming slit pore shape in addition to that by the Brunauer–Emmet–Teller method.[18] We fit the second set of data normalized with the specific surface area from NLDFT and obtained $a_0 = 0.51$ Å and $\varepsilon_r = 6.72$, which do not agree as well with our calculations and with the fact that the pore size is too small to accommodate solvated ions which would otherwise result in a higher dielectric constant. Comparing the largest capacitance in this regime with the limiting capacitance value of large pores, we find that micropores have some advantage over mesopores as indicated by Gogotsi and co-workers.[3] It is obvious that the highest capacitance value possible for micropores is determined by the size of the desolvated counterions; therefore, engineering the sizes of the electrolyte ions may further improve the energy density of nanoporous carbon supercapacitors.

There appears to be no good model for the transition region II; however, the experimental data may still be understood in light of the sizes of the desolvated/solvated ions. Data group E has higher capacitance values than group C, showing similar anomalous behavior as in group D. We speculate that data group E should be associated with EWCCs as the larger methylsulfonate ion (MS^-) dictates larger pores for the formation of EWCCs. Further experiments are indispensable to clarify this point. In comparison, the data in group F are above the extrapolated red dashed curve, implying larger ε_r values. Pores in this region are still too small to accommodate the inner cylinder of counterions, but solvated counterions can enter pores to form EWCCs, leading to a higher ε_r value coming from the (partially removed) solvation shell. Unlike region III, concentrations should not have effects on the capacitance in regions I and II for the absence of its effect on d.

Using DFT, we calculated the radial charge distribution of electrolyte ions enclosed in nanotubes to corroborate the parameter a_0 obtained from the fits described above. First, the geometries of TEA^+ (global minimum, D_{2d}), BF_4^- (T_d), MS^- (staggered conformation, C_{3v}), and a neutral "armchair" (6,6) nanotube terminated with hydrogen atoms $C_{156}H_{24}$ (labeled as a66(H), D_{6h}) were optimized with B3LYP/cc-pVDZ using the NWChem suite of programs.[19] The resulting TEA^+ and BF_4^- ions were then placed at the center of a66(H) tubes. To reduce the computational cost, the orientations of TEA^+, BF_4^-, and a66(H) were adjusted so that their symmetries are commensurate, leading to the highest possible symmetry of D_2 for TEA^+@a66(H)$^-$ and C_{2v} for BF_4^-@a66(H)$^+$, respectively. Both systems are neutral, and charge transfers take place automatically. For the pore of a66(H) with a radius of 4.1 Å, TEA^+ is too large with a radius of 3.4 Å,[20] which is about the length of an ethyl group, and TEA^+ can only enter a66(H) with its C_2' axis in alignment with the pore axis. Assuming rigid pores, we performed constrained optimizations of TEA^+@a66(H)$^-$ and BF_4^-@a66(H)$^+$ with the geometries of the tube and the centers of the inner ions fixed.

Next, the optimized geometries of TEA^+@a66(H)$^-$, BF_4^-@a66(H)$^+$, and MS^- were used to calculate the charge densities (CDs) of these systems and of neutral TEA, BF_4, a66(H), and MS. The charge-density difference for TEA^+@a66(H)$^-$ was then calculated by CD(TEA^+@a66(H)$^-$)−[CD(TEA) + CD(a66(H))], providing the locations of the electron and the hole.[21] This process was carried out for BF_4^-@a66(H)$^+$ likewise, while for MS^-, the charge-density difference was calculated by CD(MS^-)−CD(MS). The radial charge distribution of BF_4^-@a66(H)$^+$ (shown in Figure 3) was calculated from the charge-density difference

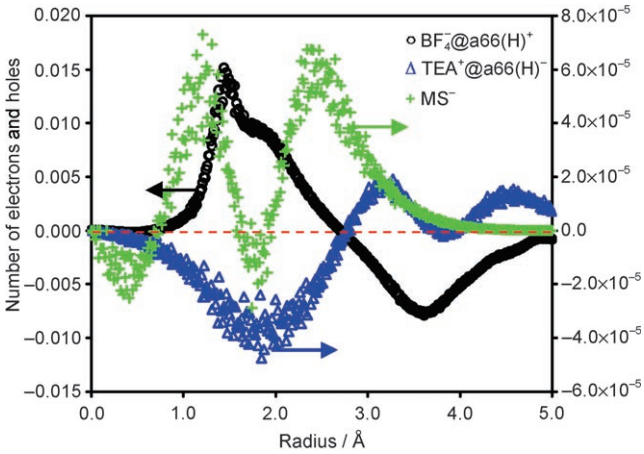

Figure 3. Radial charge distributions as a function of radius within the boron-centered sphere for BF_4^-@a66(H)$^+$, within the plane containing two terminal C atoms perpendicular to the pore axis for TEA^+@a66(H)$^-$, and within the plane of the O atoms perpendicular to the C_3 axis for MS^-. The arrows indicate the axis that is referred to.

within the boron-centered sphere on the basis of an assumption of free rotation of BF_4^- inside the pore. For TEA^+@a66(H)$^-$, we found by Mulliken population analysis that the positive charge is primarily located around the terminal methyl groups (see Table S1 in the Supporting Information), and therefore, the radical charge distribution was calculated within the plane having two terminal C atoms and perpendicular to the pore axis. Similar to TEA^+, MS^- would enter a micropore with its C_3 axis down the pore axis owing to the relatively large dimension along the C_3 axis. The radial charge distribution was calculated within the plane of the O atoms perpendicular to the C_3 axis where the negative charge is mainly located according to the Mulliken population analysis. As we can see from Figure 3, within a 3-Å radius, the curves for BF^-@a66(H)$^+$ and MS^- are positive, indicating the presence of electrons, while the curve for TEA^+@a66(H)$^-$ is negative, showing the presence of holes.

Finally, the ionic radii were estimated from Figure 3 as follows. We considered as a_0 the radius where 90% of the

charge (either electron or hole) is enclosed by integrating the curves in Figure 3, and obtained a_0 values of 2.22, 2.38, and 3.13 Å for BF_4^-, TEA^+, and MS^-, respectively. To test the effect of the enclosure of the tube a66(H), the a_0 value of BF_4^- was also calculated for its bare ion with T_d symmetry from its charge-density difference obtained in the same way as for MS^-, and we obtained an a_0 value of 2.31 Å, which is virtually the same as that calculated with BF_4^-@a66(H)$^+$. The estimated radius of BF_4^- is in excellent agreement with the literature value of 2.3 Å[20] and the fitting results. The estimated radius of TEA^+ is reduced from the literature value of 3.4 Å to 2.38 Å owing to the orientation of TEA^+ inside the pore, which also agrees with the fitting results. In comparison, the effective a_0 value of MS^- is larger, thereby explaining the observation that data group E has a larger pore size than group D. The TEAMS electrolyte constitutes an asymmetric capacitor in regions I–III, even if two electrodes have the same specific surface area.

We further comment on the kinetic process in microporous carbon materials. Gogotsi and co-workers found a reduced capacitance of microporous carbons at large discharging current densities.[3] Such behavior of reduced capacitance also exists for mesoporous carbon materials probably because of the solute diffusion process, but it is more pronounced for microporous carbons. Tamai et al.[22] found that, at smaller discharge current, the capacitances of mesoporous and microporous carbon materials are in one data group but are separated into two data groups at larger discharge current, with the capacitances of microporous carbons being reduced by a larger degree than those of mesoporous carbons. This difference should be ascribed to the following kinetic process, which plays a significant role only in region I for micropores:

$$I^{\pm} + n\,S \rightleftharpoons I^{\pm}S_n \qquad (4)$$

where I and S stand for ions and solvent molecules, respectively. A negative Gibbs free energy change favors the ion solvation process. The desolvation process contributes to the equivalent series resistance in microporous carbons but not in mesoporous carbons. Temperature should also play a role on capacitance through Equation (4). Raising the temperature may facilitate the desolvation process owing to a negative entropy change according to $\Delta G = \Delta H - T\Delta S$. Leis et al.[23] found that, for carbons that included pores smaller than 11 Å, the power density increases with temperature; for others with only pores larger than 11 Å, the power density is nearly independent of temperature. The critical pore size of 11 Å (or 10 Å in Figure 2) is characteristic of EWCCs with $TEABF_4$ as the electrolyte. For EDCCs, the effect of temperature on capacitance might be cancelled out owing to its reverse effects on d and solvent viscosity.

In summary, we have proposed a theoretical model for nanoporous carbon supercapacitors with aprotic electrolytes of acetonitrile and have presented a detailed analysis of the available experimental data in the various pore size regimes, showing for the first time significant effects of curvature on the capacitance values. The model of an EDCC (and/or EWCC) allows the supercapacitor properties to be correlated with pore size, specific surface area, Debye length, electrolyte concentration and dielectric constant, and solute ion size, and lends a support for the systematic optimization of the properties of carbon supercapacitors through experiments. This model may be generalized to carbon supercapacitors with aqueous electrolytes.

Received: August 22, 2007
Revised: October 1, 2007
Published online: December 4, 2007

Keywords: carbon · density functional calculations · mesoporous materials · supercapacitors

[1] a) B. E. Conway, *Electrochemical Supercapacitors: Scientific Fundamentals and Technological Applications*, Kluwer Academic/Plenum, New York, **1999**; b) *New Carbon Based Materials for Electrochemical Energy Storage Systems: Batteries, Supercapacitors and Fuel Cells* (Eds.: I. V. Barsukov, C. S. Johnson, J. E. Doninger, V. Z. Barsukov), Springer, Dordrecht, The Netherlands, **2006**.

[2] Reviews: a) E. Frackowiak, *Phys. Chem. Chem. Phys.* **2007**, *9*, 1774; b) A. S. Aricò, P. Bruce, B. Scrosati, J.-M. Tarascon, W. van Schalkwijk, *Nat. Mater.* **2005**, *4*, 366; c) A. G. Pandolfo, A. F. Hollenkamp, *J. Power Sources* **2006**, *157*, 11; d) M. Winter, R. J. Brodd, *Chem. Rev.* **2004**, *104*, 4245; e) A. Burke, *J. Power Sources* **2000**, *91*, 37; f) R. Kötz, M. Carlen, *Electrochim. Acta* **2000**, *45*, 2483; g) S. Sarangapani, B. V. Tilak, C.-P. Chen, *J. Electrochem. Soc.* **1996**, *143*, 3791.

[3] J. Chmiola, G. Yushin, Y. Gogotsi, C. Portet, P. Simon, P. L. Taberna, *Science* **2006**, *313*, 1760.

[4] a) Unimodal pores have a uniform pore size distribution, in contrast to multimodal pores where there are different pore sizes; b) IUPAC classifies pores into three classes: micropores are pores with diameter less than 2 nm, mesopores are 2–50 nm, and macropores are 50–100 nm; see: K. S. W. Sing, D. H. Everett, R. A. W. Haul, L. Moscou, R. A. Pierotti, J. Rouquérol, T. Siemieniewska, *Pure Appl. Chem.* **1985**, *57*, 603.

[5] See Figure S6 in reference [3], where the micropore radius was treated as the estimated double-layer thickness (d) shown in Equation (1).

[6] C. Vix-Guterl, E. Frackowiak, K. Jurewicz, M. Friebe, J. Parmentier, F. Béguin, *Carbon* **2005**, *43*, 1293.

[7] J. Gamby, P. L. Taberna, P. Simon, J. F. Fauvarque, M. Chesneau, *J. Power Sources* **2001**, *101*, 109.

[8] a) E. Lust, A. Jänes, T. Pärn, P. Nigu, *J. Solid State Electrochem.* **2004**, *8*, 224; b) C. Lin, J. A. Ritter, B. N. Popov, *J. Electrochem. Soc.* **1999**, *146*, 3639.

[9] G. Q. Lu, X. S. Zhao in *Nanoporous Materials: Science and Engineering* (Eds.: G. Q. Lu, X. S. Zhao), World Scientific, Singapore, **2004**, chap. 1.

[10] C. Liang, S. Dai, *J. Am. Chem. Soc.* **2006**, *128*, 5316.

[11] a) S. J. Gregg, K. S. W. Sing, *Adsorption, Surface Area and Porosity*, Academic, New York, **1967**, chap. 3; b) R. Evans, U. M. B. Marconi, P. Tarazona, *J. Chem. Soc. Faraday Trans. 2* **1986**, *82*, 1763.

[12] a) R. de Levie, *Electrochim. Acta* **1963**, *8*, 751; b) M. Itagaki, S. Suzuki, I. Shitanda, K. Watanabe, H. Nakazawa, *J. Power Sources* **2007**, *164*, 415; c) J. H. Jang, S. M. Oh, *J. Electrochem. Soc.* **2004**, *151*, A571.

[13] P. A. Tipler, *Physics*, Worth, New York, **1976**, p. 769.

[14] C.-M. Yang, Y.-J. Kim, M. Endo, H. Kanoh, M. Yudasaka, S. Iijima, K. Kaneko, *J. Am. Chem. Soc.* **2007**, *129*, 20.

[15] J.-F. Côté, D. Brouillette, J. E. Desnoyers, J.-F. Rouleau, J.-M. St-Arnaud, G. Perron, *J. Solution Chem.* **1996**, *25*, 1163.

[16] a) B. E. Conway, J. O'M. Bockris, I. A. Ammar, *Trans. Faraday Soc.* **1951**, *47*, 756; b) L. S. Palmer, A. Cunliffe, J. M. Hough, *Nature* **1952**, *170*, 796; c) J. Dzubiella, J.-P. Hansen, *J. Chem. Phys.* **2005**, *122*, 234706.
[17] P. I. Ravikovitch, A. Neimark, *Colloids Surf. A* **2001**, *187–188*, 11.
[18] S. Brunauer, P. Emmett, E. Teller, *J. Am. Chem. Soc.* **1938**, *60*, 309.
[19] E. Apra, et al. "NWChem, A Computational Chemistry Package for Parallel Computers, Version 4.7", **2005**, Pacific Northwest National Laboratory, Richland, Washington 99352–0999, USA; see the Supporting Information.
[20] a) M. Ue, *J. Electrochem. Soc.* **1994**, *141*, 3336; b) H. D. B. Jenkins, K. P. Thakur, *J. Chem. Educ.* **1979**, *56*, 576; c) W. R. Fawcett, M. Fedurco, M. Opallo, *J. Phys. Chem.* **1992**, *96*, 9959.
[21] V. Meunier, B. G. Sumpter, *J. Chem. Phys.* **2005**, *123*, 024705.
[22] See Figures 4–6 in H. Tamai, M. Kouzu, M. Morita, H. Yasuda, *Electrochem. Solid-State Lett.* **2003**, *6*, A214.
[23] J. Leis, M. Arulepp, A. Kuura, M. Lätt, E. Lust, *Carbon* **2006**, *44*, 2122.

